Anisotropy of the Stone-Wales defect and warping of graphene nanoribbons: A first-principles analysis

Somnath Bhowmick*
Materials Research Center, Indian Institute of Science, Bangalore, India

Umesh V. Waghmare†
Jawaharlal Nehru Centre for Advanced Scientific Research (JNCASR), Bangalore, India

(Received 25 November 2009; revised manuscript received 1 March 2010; published 6 April 2010)

Stone-Wales (SW) defects, analogous to dislocations in crystals, play an important role in mechanical behavior of sp^2-bonded carbon based materials. Here, we show using first-principles calculations that a marked anisotropy in the interaction among the SW defects has interesting consequences when such defects are present near the edges of a graphene nanoribbon: depending on their orientation with respect to edge, they result in compressive or tensile stress, and the former is responsible to depression or warping of the graphene nanoribbon. Such warping results in delocalization of electrons in the defect states.

DOI: 10.1103/PhysRevB.81.155416 PACS number(s): 61.46.−w, 61.48.De, 62.25.−g, 71.15.Mb

I. INTRODUCTION

Graphene, a two-dimensional (2D) allotrope of carbon, is the motherform of all its graphitic forms. Graphene shows several fascinating electronic-transport properties, originating from the linear energy dispersion near the high-symmetry corners of the hexagonal Brillouin zone, which results in effective dynamics of electrons similar to massless Dirac Fermions.[1] But graphene is a zero band gap semiconductor,[2] which limits its applications in electronic devices. In the bulk form, a band gap can be opened up and tuned by doping graphene with boron or nitrogen[3] or by introducing uniaxial strain.[4,5] In graphene nanoribbons (GNRs), this can be accomplished using the geometry of the edges: while a GNR with a zigzag edge (ZGNR) has a vanishing gap (which opens up due to magnetic ordering), a GNR with an armchair edge (AGNR) (Ref. 6) has a nonzero gap. GNRs can be very useful for practical purposes because their band gap can be tuned by changing the ribbon width.[6] Magnetic ground state of pristine ZGNR can be exploited to explore graphene based spintronics.[7]

For any technological applications of graphene, understanding of its structural stability and mechanical behavior is crucial. For example, deviation from the perfectly planar structure in the form of ripples or wrinkles observed in graphene[8,9] can have interesting effects on electronic properties. GNRs are known to be susceptible to structural instabilities at the edges and reconstructions.[10–17] Topological defects in the honeycomb carbon lattice, such as Stone-Wales (SW) defects (pairs of pentagons and heptagons created by 90° rotation of a C-C bond[18]) occur in graphene[19] and are relevant to its structural and mechanical behavior.[20,21] It is important to understand how atomic and electronic structure of quasi-one-dimensional (1D) GNRs is influenced by such defects. In this work, we focus on the effects of the SW defects on structural stability, electronic, and magnetic properties of GNRs.

Deprived of a neighbor, an atom at the edge of GNR has a dangling bond resulting in an edge compressive stress, which can be relieved by warping, as analyzed by Shenoy *et al.*[10] using a classical potential and interpreted with a continuum model. Huang *et al.*,[11] on the other hand, found using first-principles quantum-mechanical simulations that such graphene with dangling bonds at the edges would rather undergo SW mediated edge reconstructions to relieve stresses and consequently have a flat structure. Alternatively, edge stresses in GNRs can be relieved if the dangling bonds are saturated with hydrogen (H-GNR), stabilizing the planar structure relative to the warped one.[11] How SW defect would influence the structure of a H-GNR is not clear and we uncover this in the present work. Although SW defects cost energy,[22] they do occur in graphene[19] and are shown here to *induce warping instability* even in H-GNRs.

We organize the paper in the following manner. First, we briefly describe computational details in Sec. II. A discussion follows on various stresses associated with a SW defect in bulk graphene in Sec. III A. We correlate the results obtained in this section to the mechanical properties of edge reconstructed (by SW defects) GNRs. Next, in Sec. III B, we investigate the properties of such GNRs: first the issue of structural stability in Sec. III B 1, followed by their electronic properties in Sec. III B 2. We conclude the paper in Sec. IV.

II. METHOD

We use first-principles calculations as implemented in the PWSCF code,[23] with a plane-wave basis set and ultrasoft pseudopotential, and electron exchange-correlation is treated with a local-density approximation (LDA) (Perdew-Zunger functional). In the literature, we find use of both LDA (Ref. 6) and generalized gradient approximation (GGA) (Ref. 11) in the study of properties of graphene nanoribbons, and we expect that the choice of exchange-correlation functional should not affect the main findings of our work much. We use an energy cutoff for the plane-wave basis for wave functions (charge density) of 30 (240) Ry. Nanoribbons are simulated using a supercell geometry, with a vacuum layer of >15 Å between any two periodic images of the GNR. A k-point grid of 12 (24) $\times 1 \times 1$ k points (periodic direction of

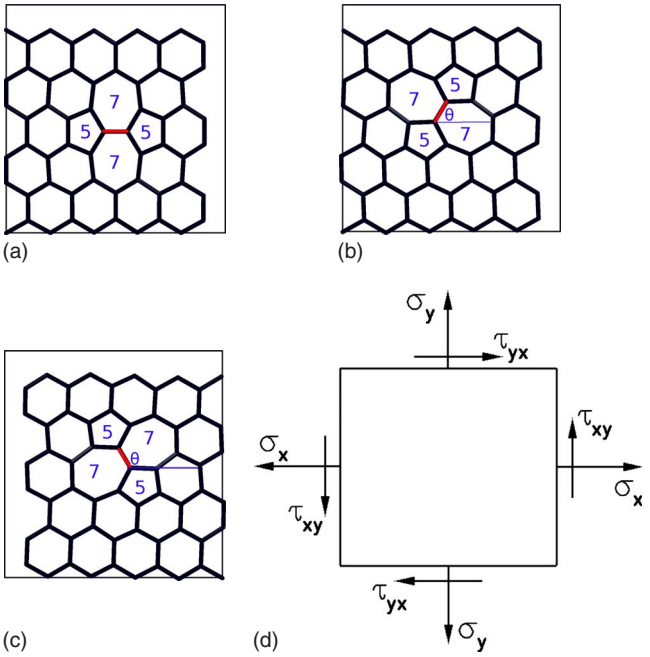

FIG. 1. (Color online) Stone Wales defect in bulk graphene; (a) $SW_{\parallel}$, (b) $SW_{\angle}$ ($\theta=60°$), (c) $SW_{\angle}$ ($\theta=120°$), where θ is the angle of the bond [rotated to create the defect, marked in red (light gray in the grayscale)] with the horizontal axis in the anticlockwise direction. (d) Planar stresses acting on the supercell.

the ribbon along x axis) is used for sampling Brillouin zone integrations for AGNR (ZGNR).

Despite many-body effects in graphene being a subject of active research, most of the current experiments support validity of band structure point of view. Results of density-functional theory (DFT) calculations are also found to be in remarkable agreement with those of the Hubbard model,[24] which takes into account onsite electron-electron interactions. While we believe that many-body effects will not drastically alter our results for structure and energetics of Stone-Wales defects and associated warping, it would indeed be an interesting research problem to analyze electronic transport properties with many body corrections, which will not be addressed in this paper.

III. RESULTS AND DISCUSSION

A. SW defects in bulk graphene

We first develop understanding of the stresses associated with SW defects in *bulk* graphene [supercells shown in Figs. 1(a)–1(c)], and we also benchmark our methodology through comparison with earlier works. The rotated bond that creates the SW defect (located at the center of the 5757 ring, marked in red, appearing light gray in the gray scale) makes an angle θ with the horizontal axis (x axis). Based on θ, we classify the defects as parallel ($\theta=0°$) and angled ($\theta\neq 0°$) and denote by the symbol $SW_{\parallel}$ [see Fig. 1(a)] and $SW_{\angle}$ [see Figs. 1(b) and 1(c)]. We express normal (shear) stress by $\sigma(\tau)$. We use +ve (−ve)σ to denote compressive (tensile) stress. For bulk graphene, the stresses are in the units of eV/Å^2 obtained by multiplying the stress tensor components with the supercell length along z direction. We show the direction of planar stresses acting on a graphene supercell in Fig. 1(d). For $SW_{\parallel}$ defect, σ_x, σ_y, and τ_{xy} are 0.40, −0.27, and 0 eV/Å^2, respectively. Under rotation θ, stress tensor components transform as

$$\sigma_x(\theta) = \frac{1}{2}(\sigma_x+\sigma_y) + \frac{1}{2}(\sigma_x-\sigma_y)\cos 2\theta + \tau_{xy}\sin 2\theta,$$

$$\sigma_y(\theta) = \frac{1}{2}(\sigma_x+\sigma_y) - \frac{1}{2}(\sigma_x-\sigma_y)\cos 2\theta - \tau_{xy}\sin 2\theta,$$

$$\tau_{xy}(\theta) = -\frac{1}{2}(\sigma_x-\sigma_y)\sin 2\theta + \tau_{xy}\cos 2\theta. \quad (1)$$

When $\theta=60°$, σ_x, σ_y, and τ_{xy} are −0.10, 0.23, and −0.29 eV/Å^2, respectively. $SW_{\angle}$ with $\theta=120°$ is same as $\theta=60°$ in terms of stresses, barring the fact that τ_{xy} has opposite sign. The energy cost for a single defect formation in a 60 atom supercell is 5.4 eV (4.8 eV) for $SW_{\parallel}$ ($SW_{\angle}$), which is in good agreement with Ref. 22. The energy difference is due to sizeable long range *anisotropic* interactions between the defects (periodic images) and can be understood in the framework of Ref. 25.

GNRs are obtained by cutting the bulk graphene sheet along certain direction—along $x(y)$ to create ZGNR (AGNR) (see Fig. 1) and the respective direction becomes the ribbon axis. Based on the analysis presented in the previous paragraph, we can readily predict the nature (sign) of stresses generated by SW defects in a GNR along the ribbon axis and in the transverse direction (i.e., along the ribbon width). However, due to finite thickness, a GNR has the freedom to relax stress along the width by deformation (expansion or contraction depending on the sign of stress). We find that, in a properly relaxed SW reconstructed GNR, except the normal stress acting along the ribbon axis, all the other stress tensor components are negligible. Thus, post structural relaxation, compressive (tensile) stress along the ribbon axis remains the only significant term in a $SW_{\parallel}$ reconstructed ZGNR (AGNR). For $SW_{\angle}$ defect, the sign of induced stress along the ribbon axis is opposite to that of $SW_{\parallel}$.

Based on bulk results, we can also predict the elastic energy cost of SW defect formation in GNRs. Note that, normal stress created by $SW_{\parallel}$ in a particular direction is of higher magnitude than that generated by $SW_{\angle}$ defect-in x direction, $\sigma_{\parallel}/\sigma_{\angle}=4$, and in y direction, $\sigma_{\parallel}/\sigma_{\angle}=1.2$. Elastic energy cost for defect formation is proportional to the stress. Hence, in a GNR $SW_{\parallel}$ defect is energetically more expensive than $SW_{\angle}$. From the above discussion, it is evident that *orientation of the defects with respect to the ribbon axis* plays a vital role in GNRs. We investigate this and its consequences in the rest of this paper.

B. SW defects in GNRs

1. Structural stability

We first describe the nomenclature for different SW defects in GNRs. The first letter, A (armchair) or Z (zigzag),

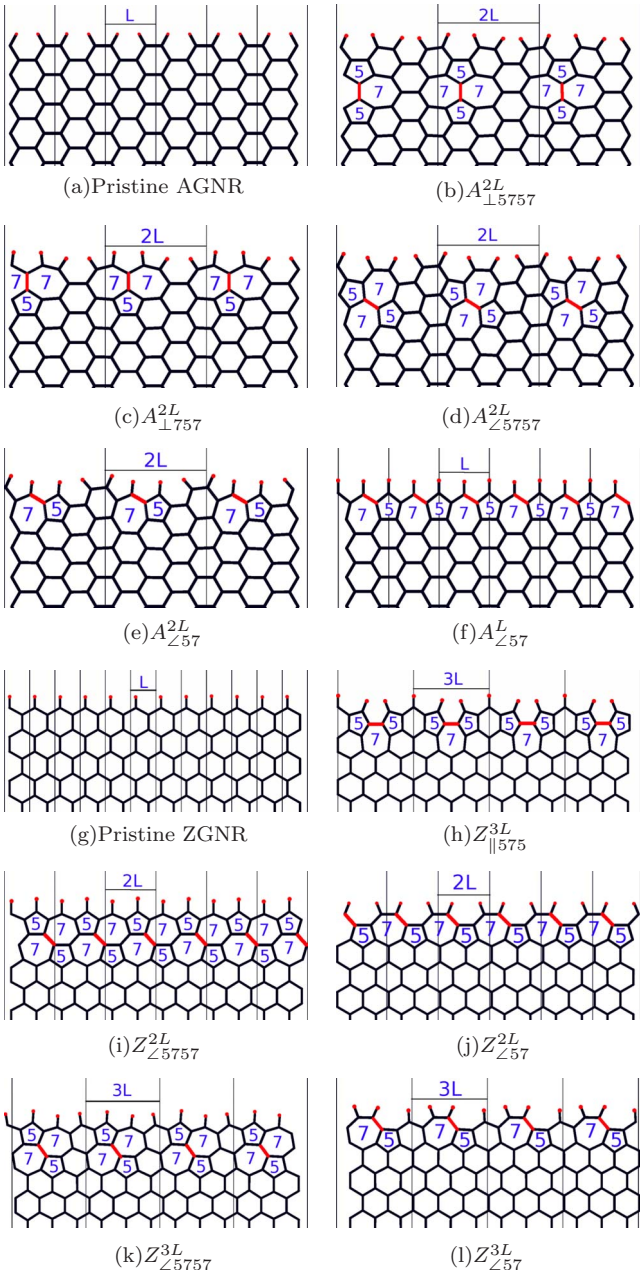

FIG. 2. (Color online) (a) Pristine AGNR and (b)–(f) SW reconstructed AGNRs. (g) Pristine ZGNR and (h)–(l) SW reconstructed ZGNRs. Red, appearing light gray in the grayscale, dots, and lines denote the hydrogen atoms and bonds rotated to create SW defects, respectively.

denotes the kind of pristine GNR hosting a SW defect, and the first subscript denotes the orientation of SW defect, defined as the angle between the rotated bond and the ribbon axis. Three possible orientations are $\parallel(\theta=0°)$, $\perp(\theta=90°)$, and $\angle$ $(\theta\neq 0°$ or $\neq 90°)$. The $SW_{\parallel}$ defect in bulk graphene described earlier falls into two categories in GNRs, $\perp$ and $\parallel$, to mark its orientation with AGNR and ZGNR edge, respectively. The series of 5s and 7s in the subscript represent constituent rings of a single defect—pentagons and heptagons. For example, a $\perp$ defect, with a pair of pentagons and heptagons each in an AGNR is denoted as $A_{\perp 5757}$ [see Fig. 2(b)]. Such a defect is away from GNR edges and keeps the armchair (or zigzag) edge shapes undisturbed [see Figs. 2(b), 2(d), 2(i), and 2(k)]. Lesser number of pentagons or heptagons (575 or 57) in the subscript implies defects overlapping with the edge and reconstructed edge shapes typically differ from that of pristine GNRs [see Figs. 2(c), 2(e), 2(f), 2(h), 2(j), and 2(l)]. The superscript denotes the length of periodicity along the ribbon axis. $L=3d(\sqrt{3}d)$ for AGNR (ZGNR), where d is the C-C bond length. Finally, a subscript w is used to differentiate warped ribbons from planar ones. All the GNRs reported here have H-terminated edges, shown by red dots in Fig. 2.

We characterize GNRs with two properties: edge formation energy per unit length and stress along the ribbon axis. The numerical values calculated using first-principles method are reported in Table I. Edge formation energy per unit length is

$$E_{edge}=\frac{1}{2L}\left(E_{GNR}-N_C E_{bulk}-\frac{N_H}{2}E_{H_2}\right), \tag{2}$$

where E_{GNR}, E_{bulk}, and E_{H_2} are the total energies of the nanoribbon supercell, one carbon atom in bulk graphene and of the isolated H_2 molecule, respectively; $N_C(N_H)$ are the number of carbon (hydrogen) atoms in the supercell. Stress reported here is $\sigma=(bc)\sigma_x$, where σ_x is the component of stress tensor along x (ribbon axis) and b and c are the supercell sizes in y and z direction. Other components of the stress tensor are negligible. E_{edge} is found to be much higher for ZGNR (0.10 eV/Å) than compared to AGNR (0.04 eV/Å). Our numbers are slightly overestimated with respect to the reported values of 0.08 eV/Å (0.03 eV/Å) for ZGNR (AGNR) (Ref. 14) obtained using the Perdew-Burke-Ernzerhof (PBE) functional (a GGA functional) for exchange-correlation energy.

Edge defects, consisting of fewer number of pentagons and/or heptagons, require less formation energy. For example, consider $A^{2L}_{\angle 5757}$ and $A^{2L}_{\angle 57}$, for which E_{edge} values are 0.51 and 0.40 eV/Å, respectively. This is true for all SW reconstructed GNRs if we compare the cases with defects of a particular orientation (see Table I). For varied orientations, $\angle$SW defects require less formation energy than compared to $\perp$ and $\parallel$ ones. For example, E_{edge} of $A^{2L}_{\angle 5757}$ is lower by 0.11 eV/Å than that of $A^{2L}_{\perp 5757}$ (consult Table I for more such instances). This observation is consistent with the argument based on our analysis of SW defect in bulk graphene. Note that ribbons with higher linear defect density (η) have higher E_{edge} and the above comparisons are meaningful only for edge reconstructed GNRs of similar η.

Defect orientations with respect to the ribbon edges control the sign of stress induced. Note that the sign of stress along the ribbon axis reported in Table I matches with the predictions based on our analysis of SW defect in bulk graphene. The ribbon widths (W) vary in the range of 18.8–20.1 Å for AGNRs and 14.4–16.1 Å for ZGNRs. This is due to the stress relaxation via deformation in the direction perpendicular to the ribbon axis. For example, an unrelaxed $A^{2L}_{\perp 5757}$ experiences compressive stress along the width and relieves it by expansion in that direction; thus

TABLE I. Linear density of defects η (number of SW defects per unit length), edge formation energy E_{edge}, stress σ along the ribbon axis, and width W of various GNRs.

GNR	η (/Å)	E_{edge} (eV/Å)	σ (eV/Å)	W (Å)	GNR	η (/Å)	E_{edge} (eV/Å)	σ (eV/Å)	W (Å)
AC	0	0.04	0	19.5	Z	0	0.10	0	15.5
$A^{2L}_{\perp 5757}$	0.12	0.62	−11	20.1	$Z^{3L}_{\parallel 575}$	0.14	0.86	19	15.0
$A^{2L}_{\perp 757}$	0.12	0.51	−11	20.0	$Z^{3L}_{\parallel 575w}$	0.14	0.70	7	14.8
$A^{2L}_{\angle 5757}$	0.12	0.51	10	19.3	$Z^{2L}_{\parallel 557}$	0.21	1.66	29	14.8
$A^{L}_{\angle 57}$	0.24	0.86	18	18.9	$Z^{2L}_{\parallel 557w}$	0.21	1.39	8	14.4
$A^{L}_{\angle 57w}$	0.24	0.81	11	18.8	$Z^{3L}_{\angle 5757}$	0.14	0.49	−5	15.9
$A^{2L}_{\angle 57}$	0.12	0.40	7	19.3	$Z^{2L}_{\angle 5757}$	0.21	0.53	−6	16.0
$A^{2L}_{\angle 57w}$	0.12	0.36	3	19.0	$Z^{3L}_{\angle 57}$	0.14	0.34	−4	16.0
					$Z^{2L}_{\angle 57}$	0.21	0.37	−5	16.1

making it slightly wider than the pristine AGNR (consult Table I). Similarly, relaxation of the tensile stress along the width by contraction makes a SW reconstructed GNR narrower than pristine GNRs (see Table I).

In contrast to the in-plane deformation to relax normal stress along the width, the only way to partially release the normal stress along ribbon axis is by an out-of-plane deformation bending. It has been reported that pristine GNRs with dangling bonds relax the compressive stress by spontaneous warping.[10] As shown in Fig. 3, we also find that SW reconstructed GNRs under compressive stress [$\angle$ ($\parallel$) in AGNR (ZGNR)] relax by local warping. For example, $\sigma(E_{edge})$ is smaller by 4(0.04) eV/Å in $A^{2L}_{\angle 57w}$ than its planar form $A^{2L}_{\angle 57}$ (see Table I for more such instances). On the other hand, SW

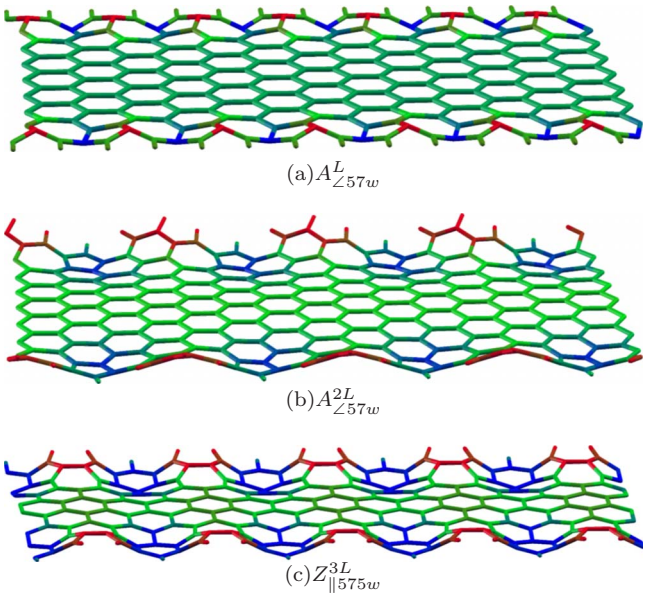

(a) $A^{L}_{\angle 57w}$

(b) $A^{2L}_{\angle 57w}$

(c) $Z^{3L}_{\parallel 575w}$

FIG. 3. (Color online) Warped structure of various different edge reconstructed nanoribbons. Red, green, and blue represent elevated "flat" and depressed regions, respectively. In grayscale, light and dark gray represents "flat" and warped regions, respectively. Atoms of a warped GNR are labeled as "flat" if $|z|<0.1$ Å, z being the height of the constituent carbon atoms. For a GNR of strictly flat geometry, $z=0$ for all the carbon atoms.

reconstructed GNRs under tensile stress [$\perp(\angle)$ in AGNR (ZGNR)] favor planar structure. In this regard, our results are in agreement with those of Ref. 11, where authors have considered only the SW defects generating tensile stress and found them to stabilize the planar geometry.

Our results for the edge reconstructions in $Z_{\angle 57}$ agree well with earlier work:[14] our estimate of E_{edge} (0.37 eV/Å) for $Z^{2L}_{\angle 57}$ is slightly higher than the PBE (a GGA exchange-correlation functional) estimate (0.33 eV/Å) of Ref. 14. However, we predict here qualitatively different types of reconstructions in $A_{\angle 57}$ and $Z_{\parallel 575}$ accompanied by warping of H-GNRs, which originate from different orientations of the SW defects. The gain in energy by H saturation of dangling bonds at the edges of a GNR is so large that even after the creation of a relatively costly SW defect, it remains lower in energy than the GNRs (no H saturation) studied in Ref. 11 (a set of DFT calculations, but the authors did not specify the exchange-correlation functional). For example, SW reconstructions at the edges (with dangling bonds) lead to a energy gain of 0.01(0.18) eV/Å for AGNR (ZGNR).[11] In contrast, we find SW reconstruction of H-GNRs *costs* 0.32(0.24) eV/Å energy in AGNR (ZGNR) at least. However, because the edge energies of pristine H-GNR and GNRs with dangling bonds are of the order of 0.1 and 1.0 eV/Å, respectively, E_{edge} of the edge reconstructed H-GNRs presented here (0.36 and 0.34 eV/Å for AGNR and ZGNR) is much smaller than that (0.99 and 0.97 eV/Å for AGNR and ZGNR) reported in Ref. 11.

So far, we have presented theoretical analysis of Stone-Wales defects in GNRs with a fixed width (19.5 and 15.5 Å for pristine AGNR and ZGNR, respectively). Since interactions among the SW defects are long ranged in nature, it will be interesting to verify how our findings depend on the width of a GNR. E_{edge} and σ for edge reconstructed ribbons of widths 20.7 and 16.9 Å and for pristine AGNR and ZGNR, respectively, are found to be almost the same as values reported in Table I for GNRs with smaller width. Specifically, our estimates of E_{edge} and σ for $A^{L}_{\angle 57w}$ type of edge reconstruction are 0.80 and 11 eV/Å, respectively for wider ribbons. Changes in E_{edge} with width of a GNR are similar to those in a pristine GNR. Despite long-ranged interactions among the SW defects, such remarkable insensitivity to

width can be understood in terms of defect concentration along the ribbon length vs width. Since defects are located at the edges, distance between the two adjacent defects along the width is 15–20 Å (see the *W* column of Table I). On the other hand, interdefect distance along the ribbon length is about 4–8 Å (inverse of the number reported in the η column of Table I). Thus, defect-defect interactions along the length of the ribbon are dominant, explaining relatively weak dependence of edge properties on the width. We note that the GNRs used in experiments are typically wider than the ones we studied here, and thus our results for edge reconstruction and related phenomena should hold good in such cases.

The ribbon periodicity (L, corresponding to minimum E_{edge} and σ in pristine GNRs) was kept fixed in our analysis, as reported in Table I. As shown in Fig. 3, for certain types of SW reconstructions, buckling relieves σ partially and reduce E_{edge}. Nevertheless, there is a small remanant stress, which could be relieved further by allowing the ribbons to relax along the periodic axis. For example, E_{edge} and σ decreases to 0.57 and 1.0 eV/Å, respectively, upon relaxation of the periodic length of ribbon $Z^{3L}_{\|575w}$. This results in an expansion of the ribbon by 4% along its length. Warping still prevails, though with slightly smaller amplitude and longer wavelength. Thus our results do not change qualitatively. We note that relaxation of the periodicity of a GNR involves (a) an elastic energy cost associated with straining of the bulk (central part) of the ribbon and (b) a small energy gain associated with relief of compressive stress at the edges. The former would dominate in wide ribbons typically used in experiments, and our results obtained without such relaxation are more relevant to experimental measurements.

Comparing the E_{edge} values from Table I, we conclude that among the edge reconstructed GNRs: warped AGNRs and flat ZGNRs are energetically more favorable than flat AGNRs and warped ZGNRs. In H-unsaturated GNRs, at an optimal concentration, SW reconstructions lower the edge energy.[11] We also find that E_{edge} values decrease on reducing the linear defect density η (by embedding SW defect in a longer supercell). However, our study is limited to a region of high η only. Whether there exists an optimal η in H-saturated GNRs also or not, at which reconstructed edge has lower energy than pristine edge, needs to be investigated and is outside the scope of the present paper.

2. Electronic properties

Electronic properties of GNRs are sensitive to the geometry of the edges at the boundary. For example, pristine AGNRs are semiconducting—the band gap arises due to quantum confinement and depends on the width of the ribbon.[6] Pristine ZGNRs also exhibit gapped energy spectrum although of entirely different origin. Gap arises due to a localized edge potential generated by edge magnetization.[6] It is well known that presence of defects or disorders at the edges can change the electronic, magnetic, and transport properties of GNRs to various extent.[27,28] In 2D graphene, topological defects such as dislocations or SW defects give rise to electronic states localized at the defect sites.[20] Presence of any such defect induced states near the edges of the SW reconstructed GNRs can have interesting consequences on their electronic and transport properties.

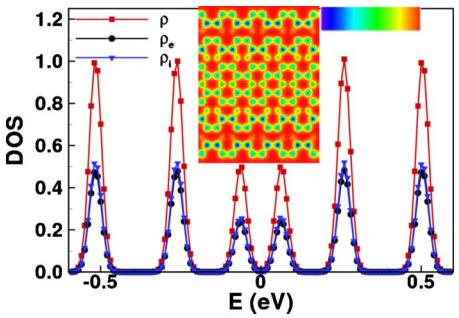

FIG. 4. (Color online) DOS and STM image of pristine AGNR visualized with XCRYSDEN (Ref. 26). $E=0$ denotes the Fermi energy. We have applied a thermal broadening equivalent to room temperature to plot the DOS in this figure and throughout the rest of the paper. Consult text for the definition of ρ, ρ_e, and ρ_i. The horizontal bar represents the color scale used in the STM image. The image has been simulated for a sample bias of −0.3 eV and reflects the spatial distribution of the local-density of states LDOS below Fermi energy.

In this section, we analyze electronic properties using the density of states (DOS) and simulated scanning tunneling microscope (STM) images of pristine and edge reconstructed GNRs. We decompose total DOS (ρ) into the sum of projected DOS of atoms located at the interior of the ribbon (ρ_i) and atoms near the edges (ρ_e). ρ_e is the sum of projected DOS of first two layers of atoms from both the edges. Since the defects are located at the edges, this technique clearly uncovers the difference between electronic band structures of a pristine and edge reconstructed GNR. Note (Fig. 3) that this is the region which undergoes warping (remains flat) if the ribbon edges are under compressive (tensile) stress. ρ_i includes the projected DOS of rest of the atoms (located in the region of the nanoribbon that always remains flat). Depending on the sample bias, STM images help identify the spatial distribution of local DOS (LDOS) below (−ve bias) and above (+ve bias) the Fermi level ($E_F=0$). These images should be useful in experimental characterization of GNRs as well as understanding consequences of such defects and warping to electronic transport in GNRs.

The DOS for a 19.5 Å wide pristine AGNR of band gap 0.1 eV (Fig. 4) shows that both ρ_i and ρ_e contributes to the ρ with equal weight and symmetric about E_F. This symmetry is known as particle-hole symmetry. The inset of Fig. 4 shows that for a sample bias of −0.3 eV, the occupied LDOS is spread over the entire ribbon. We do not present the corresponding image for a positive sample bias, which is very similar due to the underlying particle-hole symmetry.

Edge reconstruction by $\perp$SW defect (7-5-7 defect) breaks the particle-hole symmetry and a sharp peak of DOS appears above E_F (see Fig. 5), which has primary contribution from the edge atoms ($\rho_e > \rho_i$). The STM image (simulated with a sample bias of +0.2 eV) reveals that the unoccupied LDOS is localized at the defect sites, located very close to the ribbon edges. The STM image for a −ve sample bias (not shown here) illustrates that occupied LDOS is spatially distributed over the entire ribbon, similar to the pristine one.

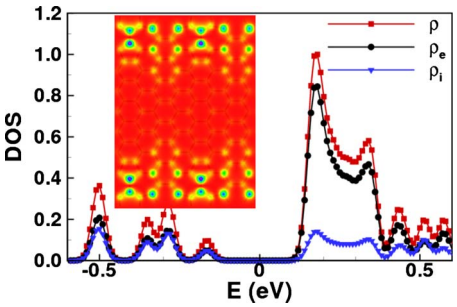

FIG. 5. (Color online) DOS and STM image of $A^{2L}_{\perp 757}$ simulated with a sample bias of +0.2 eV. The STM image shows the spatial distribution of LDOS above the Fermi energy.

Edge reconstruction by ∠SW defects (5–7 defect) have similar consequences on electronic band structure of AGNRs. A sharp peak in DOS, primarily coming from ρ_e, appears above the Fermi energy [see Fig. 6(a)]. Simulated STM image (at sample bias +0.2 eV) confirms that LDOS above the Fermi level are localized at the edges. For −ve sample bias (not presented here), occupied LDOS is spatially distributed over edge, as well as interior atoms. However, for this type of edge reconstructions, planar structure is not the stable one and the ribbon undergoes warping near the edges (see Fig. 3). As shown in Fig. 6(b), the DOS peak of edge-localized (or rather defect localized) states above the Fermi energy vanishes in the warped GNR and LDOS above E_F is spatially distributed throughout the ribbon. This is also true for LDOS below the Fermi level also (STM image not shown here). This reveals an electronic origin of the defect induced stress and its anisotropy in the localized p-like

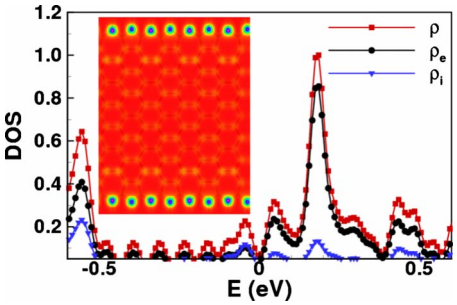

(a) $A^{L}_{\angle 57}$

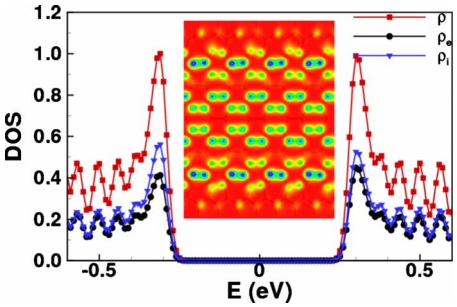

(b) $A^{L}_{\angle 57w}$

FIG. 6. (Color online) DOS and STM image of (a) $A^{L}_{\angle 57}$ and (b) $A^{L}_{\angle 57w}$. The STM images have been simulated with sample bias of +0.2 and +0.4 eV for (a) and (b), respectively. They show the spatial distribution of LDOS above the Fermi energy.

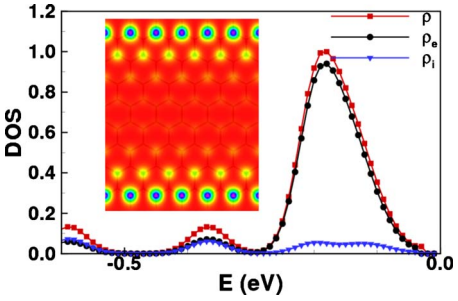

FIG. 7. (Color online) DOS up to E_F(=0.0) and STM image of pristine ZGNR simulated with a sample bias of −0.2 eV. The image illustrates the spatial distribution of LDOS below the Fermi energy.

defect state. Delocalization of this state relieves the stress and favors warping.

All the results presented here are for a pristine AGNR of narrow band gap (0.1 eV), which undergoes edge reconstructions by various SW defects. We have investigated edge reconstructions of a wide band gap AGNR also. We find qualitative similarity, such as unoccupied LDOS localized at the edges, among the edge reconstructed AGNRs of various widths and band gaps. However, the magnitude of band gap depends both on ribbon width and the type of SW reconstruction present at the edge (i.e., edge shape) and varies over a wide range of values (0.1–1 eV). The unoccupied states localized near the edges can have interesting applications in molecule detection. These states are going to act as electron acceptors and can detect some suitable electron donating molecules.

We have employed a local spin-density approximation (LSDA) in our calculations to explore the possibilities of magnetic ordering in GNRs. We initialize our calculation with atoms at the edges of GNRs to have nonzero spin polarization [of same (opposite) sign at the two edges in FM (AFM) configurations]. While the magnitude of spin at edge atoms change in the course to self-consistency, their relative signs remain the same if the corresponding magnetic ordering is stable. As mentioned earlier, pristine ZGNRs have gapped antiferromagnetic ground sate.[6,7] We illustrate the DOS and simulated STM image of a pristine ZGNR with a width of 15.5 Å in Fig. 7. The band gap is 0.3 eV and we show DOS up to the Fermi level. Note that up and down spin electrons have similar energy spectrum and are not shown separately. The STM image has been simulated for a sample bias of −0.2 eV and reveals that LDOS below the Fermi energy is localized at the zigzag edges. The edges are spin polarized—ferromagnetically coupled along a particular edge but antiferromagnetic between two opposite edges (not shown here).

We find that edge reconstructions by SW defects *destroy magnetism*. At high defect density, this leads to a *nonmagnetic metallic* ground state and at lower defect density magnetism survives with a weaker magnitude. In this paper, our investigation is restricted to the regime of high defect density [where all or most of the zigzag edges have been reconstructed by SW defects—see Figs. 2(h)–2(l)] and we do not discuss the issue of magnetism any further. The states at E_F

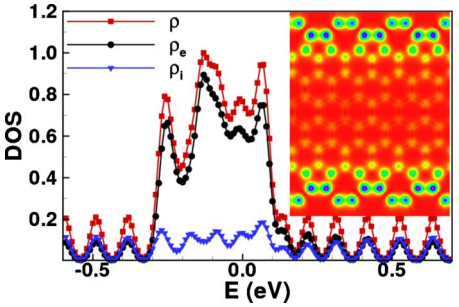

FIG. 8. (Color online) DOS and STM image of $Z^{2L}_{\angle 57}$, simulated with a sample bias of −0.2 eV. The image shows the spatial distribution of occupied LDOS.

arise primarily from the edges for all the zigzag GNRs.

The DOS and simulated STM image (bias voltage −0.2 eV) of a ∠SW (5–7 defect) edge reconstructed ZGNR (see Fig. 8) reveal a nonzero DOS at E_F(=0) and that the ground state is of a nonmagnetic metal. The STM image shows the formation of nearly isolated dimers along the edge. Reconstruction of ZGNR edge by ∥SW defect (5-7-5 defect) does not alter the electronic properties qualitatively. Such ZGNRs are also nonmagnetic metallic with planar as well as warped geometries (not shown here). However, these are very high energy edges and are unlikely to be preferred over 5–7 SW reconstructions in ZGNRs. The 5–7 defects can act as interface of hybrid graphene and hybrid GNRs, having both armchair and zigzaglike features. Such materials have remarkable electronic and magnetic properties.[29]

IV. CONCLUSION

In conclusion, the sign of stress induced by a SW defect in a GNR depends on the orientation of the SW defect with respect to the ribbon edge, and the relaxation of the structure to relieve this stress drives its stability. Local warping or wrinkles arise in the GNR when the stress is compressive, while the structure remains planar otherwise. The specific consequences to AGNR and ZGNR can be understood from the anisotropy of the stress induced by a SW defect embedded in bulk graphene. Using the analogy between a SW defect and a dislocation, it should be possible to capture the interaction between a SW defect in the interior of a GNR and its edge within a continuum framework that includes images of SW defects in the edges. As the images of SW defects are also SW defects, their interactions can be readily captured within the continuum framework of Ref. 25. Our work shows how warping of GNRs can be nucleated at the SW defects localized at the edges and be responsible for flakelike shapes of graphene samples seen commonly in experiments. Such warping results in delocalization of electrons in the defect states. In ZGNRs, magnetic ordering weakens due to the presence of SW defects at the edges and the ground state is driven towards that of a nonmagnetic metal.

ACKNOWLEDGMENTS

S.B. thanks Vijay B. Shenoy for valuable discussions, suggestions, and comments. U.V.W. acknowledges support from an IBM Faculty award.

*bsomnath@mrc.iisc.ernet.in
†waghmare@jncasr.ac.in

[1] A. H. Castro Neto, F. Guinea, N. M. R. Peres, K. S. Novoselov, and A. K. Geim, Rev. Mod. Phys. **81**, 109 (2009).
[2] P. R. Wallace, Phys. Rev. **71**, 622 (1947).
[3] L. S. Panchakarla, K. S. Subrahmanyam, S. K. Saha, A. Govindaraj, H. R. Krishnamurthy, U. V. Waghmare, and C. N. R. Rao, Adv. Mater. (Weinheim, Ger.) **21**, 4726 (2009).
[4] Z. H. Ni, T. Yu, Y. H. Lu, Y. Y. Wang, Y. P. Feng, and Z. X. Shen, ACS Nano **2**, 2301 (2008).
[5] Z. H. Ni, H. M. Wang, Y. Ma, J. Kasim, Y. H. Wu, and Z. X. Shen, ACS Nano **2**, 1033 (2008).
[6] Y. W. Son, M. L. Cohen, and S. G. Louie, Phys. Rev. Lett. **97**, 216803 (2006).
[7] Y. W. Son, M. L. Cohen, and S. G. Louie, Nature (London) **444**, 347 (2006).
[8] J. C. Meyer, A. K. Geim, M. I. Katsnelson, K. S. Novoselov, T. J. Booth, and S. Roth, Nature (London) **446**, 60 (2007).
[9] A. Fasolino, J. H. Los, and M. I. Katsnelson, Nature Mater. **6**, 858 (2007).
[10] V. B. Shenoy, C. D. Reddy, A. Ramasubramaniam, and Y. W. Zhang, Phys. Rev. Lett. **101**, 245501 (2008).
[11] B. Huang, M. Liu, N. Su, J. Wu, W. Duan, B. L. Gu, and F. Liu, Phys. Rev. Lett. **102**, 166404 (2009).
[12] K. V. Bets and B. I. Yakobson, Nano Res. **2**, 161 (2009).
[13] P. Koskinen, S. Malola, and H. Häkkinen, Phys. Rev. Lett. **101**, 115502 (2008).
[14] T. Wassmann, A. P. Seitsonen, A. M. Saitta, M. Lazzeri, and F. Mauri, Phys. Rev. Lett. **101**, 096402 (2008).
[15] P. Koskinen, S. Malola, and H. Hakkinen, arXiv:0906.0688 (unpublished).
[16] C. O. Girit *et al.*, Science **323**, 1705 (2009).
[17] M. H. Gass, U. Bangert, A. L. Bleloch, P. Wang, R. R. Nair, and A. K. Geim, Nat. Nanotechnol. **3**, 676 (2008).
[18] A. J. Stone and D. J. Wales, Chem. Phys. Lett. **128**, 501 (1986).
[19] J. C. Meyer, C. Kisielowski, R. Erni, M. D. Rossell, M. F. Crommie, and A. Zettl, Nano Lett. **8**, 3582 (2008).
[20] A. Carpio, L. L. Bonilla, F. de Juan, and M. A. H. Vozmediano, New J. Phys. **10**, 053021 (2008).
[21] B. I. Yakobson and P. Avouris, Top. Appl. Phys. **80**, 287 (2001).
[22] M. T. Lusk and L. D. Carr, Phys. Rev. Lett. **100**, 175503 (2008).
[23] P. Giannozzi, http://www.quantum-espresso.org
[24] J. Fernández-Rossier and J. J. Palacios, Phys. Rev. Lett. **99**, 177204 (2007).
[25] E. Ertekin, D. C. Chrzan, and M. S. Daw, Phys. Rev. B **79**, 155421 (2009).
[26] A. Kokalj, J. Mol. Graphics Modell. **17**, 176 (1999).
[27] H. Kumazaki and D. S. Hirashima, J. Phys. Soc. Jpn. **77**, 044705 (2008).
[28] G. Schubert, J. Schleede, and H. Fehske, Phys. Rev. B **79**, 235116 (2009).
[29] A. R. Botello-Mendez, E. Cruz-Silva, F. Lopez-Urias, B. G. Sumpter, V. Meunier, M. Terrones, and H. Terrones, ACS Nano **3**, 3606 (2009).